

A Four-Pixel Scheme for Singular Differential Equations

Martin Welk¹, Joachim Weickert¹, and Gabriele Steidl²

¹ Mathematical Image Analysis Group
Faculty of Mathematics and Computer Science, Bldg. 27
Saarland University, 66041 Saarbrücken, Germany
{welk,weickert}@mia.uni-saarland.de
<http://www.mia.uni-saarland.de>

² Faculty of Mathematics and Computer Science, D7, 27
University of Mannheim, 68131 Mannheim, Germany
steidl@math.uni-mannheim.de
<http://kiwi.math.uni-mannheim.de>

Abstract. Singular diffusion equations such as total variation (TV) and balanced forward–backward (BFB) diffusion are appealing: They have a finite extinction time, and experiments show that piecewise constant structures evolve. Unfortunately, their implementation is awkward. The goal of this paper is to introduce a novel class of numerical methods for these equations in the 2D case. They are simple to implement, absolutely stable and do not require any regularisation in order to make the diffusivity bounded. Our schemes are based on analytical solutions for 2×2 -pixel images which are combined by means of an additive operator splitting (AOS). We show that they may also be regarded as iterated 2D Haar wavelet shrinkage. Experiments demonstrate the favourable performance of our numerical algorithm.

1 Introduction

Nonlinear diffusion filters [15, 21] constitute an important class of image enhancement methods. Let $\Omega \subset \mathbb{R}^2$ denote our two-dimensional image domain and $f : \Omega \rightarrow \mathbb{R}$ an initial greyscale image. Then the idea behind nonlinear diffusion filtering is to consider $f(x)$ as initial condition

$$u(x, 0) = f(x) \quad \text{on } \Omega \tag{1}$$

of a nonlinear diffusion process

$$\partial_t u = \operatorname{div} (g(|\nabla u|) \nabla u) \quad \text{on } \Omega \times (0, \infty) \tag{2}$$

with suitable boundary conditions, e.g. the reflecting (homogeneous Neumann) boundary conditions

$$\partial_n u = 0 \quad \text{on } \partial\Omega \times (0, \infty). \tag{3}$$

Here $\nabla = (\partial_{x_1}, \partial_{x_2})^\top$ denotes the spatial nabla operator and n is the outer normal vector on the image boundary $\partial\Omega$. The resulting solution $u(x, t)$ creates a scale-space family $\{u(x, t) \mid t \geq 0\}$ of processed images, where the diffusion time t serves as scale parameter: Larger values of t give more simplified images $u(x, t)$. In order to preserve (or even enhance) edges and to simultaneously smooth within more homogeneous regions, the diffusivity function $g(|\nabla u|)$ is chosen as a decreasing nonnegative function.

While early proposals for nonlinear diffusion filters use bounded diffusivities [15, 6], more recently there has been a growing interest in unbounded diffusivities that become singular in zero [2, 9–11, 16]. Experimentally one observes that singular diffusion filters lead to piecewise constant images. This is also in accordance with theoretical results by Nikolova [14] who showed that related discrete variational approaches allow piecewise constant solutions if and only if the regulariser is nondifferentiable in zero.

As a prototype for a class of singular diffusivities we consider the family

$$g(|\nabla u|) = \frac{1}{|\nabla u|^p} \quad (p \geq 0). \quad (4)$$

These diffusivities offer the advantage that they do not require to tune any image specific contrast parameters. Moreover, they lead to scale invariant filters [1], for which even some analytical results have been established [20].

For $p = 1$ one obtains the *total variation (TV)* diffusion [2, 9], the diffusion filter that corresponds to TV minimisation [18] with a penaliser $\Psi(|\nabla u|^2) = 2|\nabla u|$. TV diffusion offers a number of interesting properties such as finite extinction time [3], shape-preserving qualities [4], and equivalence to TV regularisation in 1-D [5, 17]. For $p > 1$ the diffusion not only preserves edges but even enhances them. A diffusivity with $p = 2$ has been considered in [11] for the so-called *balanced forward-backward (BFB)* diffusion filtering.³

Although singular diffusion equations have very attractive properties, their numerical implementation is difficult. Explicit finite difference schemes are only stable for time step sizes that are inversely proportional to an upper bound for the diffusivity, while absolutely stable implicit or semi-implicit schemes lead to linear systems of equations with condition numbers that are increasing functions of this bound. As a result, iterative numerical schemes may reveal slow convergence, and in general numerical errors can be amplified. In order to limit all these problems, it is common to regularise the diffusivity function by replacing it by the bounded diffusivity

$$g(|\nabla u|) = \frac{1}{(|\nabla u|^2 + \varepsilon^2)^{p/2}}. \quad (5)$$

In this case, however, one observes that blurring artifacts are introduced and some of the nice theoretical properties of singular nonlinear diffusion filters do no longer hold.

³ While a complete well-posedness theory exists for $p \leq 1$, some theoretical questions are a topic of ongoing research for the edge-enhancing case $p > 1$.

The goal of the present paper is to address these problems by introducing a novel class of numerical schemes for singular diffusion equations. They are based on an analysis of the dynamical system that results from a space discretisation of singular diffusion filters for images with 2×2 pixels. For this scenario we are able to derive an analytical solution. It serves as a building block in a numerical scheme for general 2-D images, since we can assemble these local analytical solutions by means of an additive operator splitting (AOS) [12, 22] to a global numerical approximation. Our scheme is very simple, it is absolutely stable and reveals good rotation invariance. It does not require regularised diffusivities of type (5). Interestingly, it can also be related to a recently introduced family of shift invariant wavelet shrinkage methods with coupled shrinkage functions [13].

Our paper is organised as follows. In Section 2 we analyse space-discrete singular diffusion filters for 2×2 images, derive their analytical solutions, and relate them to Haar wavelet shrinkage of 2×2 images. These analytical solutions are used in Section 3 for constructing numerical schemes for 2-D images of arbitrary size. We analyse their stability and consistency properties, and show their equivalence to suitable shift invariant wavelet shrinkages. Numerical experiments are presented in Section 4, and the paper is concluded with a summary in Section 5.

Related work. Relations between one-dimensional discrete TV diffusion, TV regularisation and Haar wavelet shrinkage were investigated in [19]. A main instrument in studying one-dimensional total variation methods were considerations of two-pixel signals. Based on the two-pixel dynamics, a novel scheme for N -pixel TV diffusion could be established. We may regard our present work as a two-dimensional extension. The two-dimensional situation, however, turns out to be significantly more complicated than the one-dimensional scenario. With respect to TV-diminishing flows along the directions of Haar wavelets, our work can also be related to a paper by Coifman and Sowa [8]. A regularisation-free approach to TV regularisation has been proposed by Chambolle [7]. It should be noted that in our paper we consider the parabolic diffusion case instead of the elliptic regularisation setting. Moreover, we do not restrict ourselves to the TV case: Our results hold for any arbitrary singular diffusivity of type (4).

2 Analytical Results for 2×2 -Pixel Images

We start by examining the simplest nontrivial 2-D images, namely those having only 2×2 pixels. This will provide the basis of our new numerical scheme for solving singular diffusion equations on $N \times M$ -pixel images.

2.1 Nonlinear Diffusion

We consider the diffusion equation (2) for 2×2 -pixel images $u = (u_{i,j})_{i,j=1}^2$ with periodic boundary conditions and initial image $f = (f_{i,j})_{i,j=1}^2$. Due to the

periodic boundary conditions every 2×2 cell in the extended image

$$\begin{array}{c|cc|c} u_{2,2} & u_{2,1} & u_{2,2} & u_{2,1} \\ \hline u_{1,2} & u_{1,1} & u_{1,2} & u_{1,1} \\ \hline u_{2,2} & u_{2,1} & u_{2,2} & u_{2,1} \\ \hline u_{1,2} & u_{1,1} & u_{1,2} & u_{1,1} \end{array}$$

contains exactly the same pixels. This is not true for other boundary conditions, e.g., reflecting boundary conditions.

We want to find an appropriate space discretisation of (2) that results in an ordinary system of four differential equations which can be solved analytically. First we notice that in our 2×2 cell there is one distinguished location where the diffusivity can be optimally approximated, namely the midpoint of the cell. Therefore we use only the midpoint diffusivity $g := g(D(u))$ within the whole image, where

$$D(u) := \frac{1}{2} \left((u_{1,1} - u_{1,2})^2 + (u_{2,1} - u_{2,2})^2 + (u_{1,1} - u_{2,1})^2 + (u_{1,2} - u_{2,2})^2 + (u_{1,1} - u_{2,2})^2 + (u_{1,2} - u_{2,1})^2 \right)^{1/2} \quad (6)$$

denotes the discretisation of $|\nabla u|$ in the midpoint of the cell, if the grid size $h := 1$ is chosen in both directions. This discretisation is just the average of the two finite difference discretisations of $|\nabla u|$ with respect to the usual directions $x = (1, 0)^T$, $y = (0, 1)^T$ and with respect to the 45° diagonal directions $\xi = \frac{1}{\sqrt{2}}(1, 1)^T$, $\eta = \frac{1}{\sqrt{2}}(1, -1)^T$, respectively. Next, we discretise the remaining gradient and divergence of the right-hand side of $\partial_t u = \text{div}(g\nabla u)$ with respect to the same directions.

With the uniform midpoint diffusivity $g := g(D(u))$, the discretisation related to x and y leads for $i, j = 1, 2$ to

$$\dot{u}_{i,j} = g \cdot (u_{i+1,j} + u_{i-1,j} + u_{i,j+1} + u_{i,j-1} - 4u_{i,j}),$$

where the dot denotes time differentiation, and by our boundary conditions to

$$\begin{aligned} \dot{u}_{1,1} &= 2g \cdot (u_{1,2} + u_{2,1} - 2u_{1,1}), & \dot{u}_{1,2} &= 2g \cdot (u_{1,1} + u_{2,2} - 2u_{1,2}), \\ \dot{u}_{2,1} &= 2g \cdot (u_{1,1} + u_{2,2} - 2u_{2,1}), & \dot{u}_{2,2} &= 2g \cdot (u_{1,2} + u_{2,1} - 2u_{2,2}). \end{aligned}$$

The discretisation with respect to ξ and η results for $i, j = 1, 2$ in

$$\dot{u}_{i,j} = g \cdot \frac{1}{2} (u_{i+1,j+1} + u_{i-1,j-1} + u_{i+1,j-1} + u_{i-1,j+1} - 4u_{i,j})$$

and by applying the boundary conditions in

$$\begin{aligned} \dot{u}_{1,1} &= 2g \cdot (u_{2,2} - u_{1,1}), & \dot{u}_{1,2} &= 2g \cdot (u_{2,1} - u_{1,2}), \\ \dot{u}_{2,1} &= 2g \cdot (u_{1,2} - u_{2,1}), & \dot{u}_{2,2} &= 2g \cdot (u_{1,1} - u_{2,2}). \end{aligned}$$

Weighted averaging of both discretisations with weights $\alpha \in [0, 1]$ and $1 - \alpha$ gives the ordinary system of differential equations

$$\begin{aligned} \dot{u}_{1,1} &= 2g \cdot (-(1 + \alpha)u_{1,1} + \alpha u_{1,2} + \alpha u_{2,1} + (1 - \alpha)u_{2,2}), \\ \dot{u}_{1,2} &= 2g \cdot (\alpha u_{1,1} - (1 + \alpha)u_{1,2} + (1 - \alpha)u_{2,1} + \alpha u_{2,2}), \\ \dot{u}_{2,1} &= 2g \cdot (\alpha u_{1,1} + (1 - \alpha)u_{1,2} - (1 + \alpha)u_{2,1} + \alpha u_{2,2}), \\ \dot{u}_{2,2} &= 2g \cdot ((1 - \alpha)u_{1,1} + \alpha u_{1,2} + \alpha u_{2,1} - (1 + \alpha)u_{2,2}) \end{aligned} \quad (7)$$

with initial conditions $u_{i,j}(0) = f_{i,j}$, $i, j = 1, 2$. From $\dot{u}_{1,1} + \dot{u}_{1,2} + \dot{u}_{2,1} + \dot{u}_{2,2} = 0$ we see that the average grey value $\mu := \frac{1}{4}(f_{1,1} + f_{1,2} + f_{2,1} + f_{2,2})$ is preserved during the diffusion process.

In this paper, we are mainly interested in the case $\alpha = 1/2$, where system (7) further simplifies to

$$\dot{u}_{i,j} = 4g \cdot (\mu - u_{i,j}), \quad i, j = 1, 2, \quad (8)$$

which is a dynamical system with discontinuous right hand side. It is not difficult to verify that this system possesses the unique analytical solution

$$u_{i,j}(t) = \begin{cases} \mu + (1 - 4p(D(f))^{-p}t)^{1/p} (f_{i,j} - \mu), & 0 \leq t < (D(f))^p/(4p), \\ \mu, & t \geq (D(f))^p/(4p). \end{cases} \quad (9)$$

For $p = 1$, particularly, (2) is the TV diffusion equation $\partial_t u = \operatorname{div}(\nabla u/|\nabla u|)$. The analytical solution of our 2×2 -pixel version

$$u_{i,j}(t) = \begin{cases} \mu + (1 - 4t/D(f)) (f_{i,j} - \mu), & 0 \leq t < D(f)/4, \\ \mu, & t \geq D(f)/4 \end{cases} \quad (10)$$

shows a linear evolution which can be written in a slightly different form as

$$u_{i,j}(t) = f_{i,j} + (4t/D(f)) \cdot (\mu - f_{i,j}) \min\{1, D(f)/(4t)\}, \quad i, j = 1, 2. \quad (11)$$

For $p = 2$, we obtain the BFB diffusion $\partial_t u = \operatorname{div}(\nabla u/|\nabla u|^2)$. The analytical solution in the 2×2 setting reads

$$u_{i,j}(t) = \begin{cases} \mu + \sqrt{1 - 8t/(D(f))^2} (f_{i,j} - \mu), & 0 \leq t < (D(f))^2/8, \\ \mu, & t \geq (D(f))^2/8. \end{cases} \quad (12)$$

2.2 Haar Wavelet Shrinkage

In [19], it was shown that one-dimensional nonlinear diffusion on two-pixel signals coincides with Haar wavelet shrinkage if the shrinkage function is chosen in accordance with the diffusivity and the threshold parameter is equal to the diffusion time. The two-dimensional Haar wavelet transform acts naturally on subsequent 2×2 -pixel tiles of an image. Let us choose one such tile, say $f := (f_{i,j})_{i,j=1}^2$, and explain how it changes under two-dimensional Haar wavelet shrinkage. One cycle of Haar wavelet shrinkage consists of three steps. In the first step, the *analysis*

step, the low and high pass Haar filters are applied to the rows and columns of f . More precisely, f is multiplied from the left and the right by the orthogonal matrix $W := \frac{1}{\sqrt{2}} \begin{pmatrix} 1 & 1 \\ 1 & -1 \end{pmatrix}$. This results in an image $c := (c_{i,j})_{i,j=1}^2$ with

$$\begin{aligned} c_{1,1} &= \frac{1}{2}(f_{1,1} + f_{1,2} + f_{2,1} + f_{2,2}), & c_{1,2} &= \frac{1}{2}(f_{1,1} - f_{1,2} + f_{2,1} - f_{2,2}), \\ c_{2,1} &= \frac{1}{2}(f_{1,1} + f_{1,2} - f_{2,1} - f_{2,2}), & c_{2,2} &= \frac{1}{2}(f_{1,1} - f_{1,2} - f_{2,1} + f_{2,2}). \end{aligned}$$

In the second step, the *shrinkage step*, we modify the high-pass coefficients by reducing the absolute values of some or all of them. To this end, we apply a shrinkage function S_θ depending on a threshold parameter θ to the high-pass filtered coefficients, i.e. we compute $S_\theta(c_{1,2})$, $S_\theta(c_{2,1})$, $S_\theta(c_{2,2})$ and leave the low-pass coefficient $c_{1,1}$ as it is. In the third step, the *synthesis step*, we perform just the inverse transform of step 1 on the shrunken image, i.e., since $W^{-1} = W$, we multiply again from the left and the right by W and obtain

$$\begin{aligned} v_{1,1} &= \mu + \frac{1}{2}(S_\theta(c_{1,2}) + S_\theta(c_{2,1}) + S_\theta(c_{2,2})), \\ v_{1,2} &= \mu + \frac{1}{2}(-S_\theta(c_{1,2}) + S_\theta(c_{2,1}) - S_\theta(c_{2,2})), \\ v_{2,1} &= \mu + \frac{1}{2}(S_\theta(c_{1,2}) - S_\theta(c_{2,1}) - S_\theta(c_{2,2})), \\ v_{2,2} &= \mu + \frac{1}{2}(-S_\theta(c_{1,2}) - S_\theta(c_{2,1}) + S_\theta(c_{2,2})). \end{aligned}$$

In [13], the authors proposed to choose a diffusion inspired shrinkage function that simultaneously depends on $c_{1,2}$, $c_{2,1}$ and $c_{2,2}$. In contrast to the classical wavelet shrinkage, this results in an improved rotation invariance of the resulting image. We use this knowledge and define our shrinkage function in dependence on

$$D(f) = (c_{1,2}^2 + c_{2,1}^2 + c_{2,2}^2)^{1/2}.$$

It is straightforward to check that the value $D(f)$ indeed coincides with the one defined in (6). Applying the shrinkage function

$$S_\theta(s; D(f)) := \begin{cases} (1 - 4p (D(f))^{-p} \theta)^{1/p} s, & D(f) \geq (4p\theta)^{1/p}, \\ 0 & D(f) < (4p\theta)^{1/p}. \end{cases} \quad (13)$$

our Haar wavelet shrinkage produces for $i, j = 1, 2$ the values

$$v_{i,j} = \begin{cases} \mu + (1 - 4p (D(f))^{-p} \theta)^{1/p} (f_{i,j} - \mu), & D(f) \geq (4p\theta)^{1/p}, \\ \mu, & D(f) < (4p\theta)^{1/p}. \end{cases} \quad (14)$$

Comparing this equation with (9) we observe that on 2×2 pixels our Haar wavelet shrinkage with shrinkage function (13) coincides with the solution of the nonlinear diffusion equation with diffusivity (4), where the shrinkage parameter θ plays the same role as the diffusion time t .

3 A Numerical Scheme for Images of Arbitrary Size

Now we consider arbitrary $N \times M$ -pixel images $u := (u_{i,j})_{i,j=1}^{N,M}$ which are extended to the full planar grid by, e.g., reflecting boundary conditions.

3.1 Numerical Scheme for Nonlinear Diffusion

We discretise the diffusion equation (2) in space again with respect to the x - y and ξ - η directions. Approximating gradient and divergence by finite differences in x and y directions leads to

$$\begin{aligned} \operatorname{div}(g(|\nabla u|)\nabla u)_{i,j} &\approx g_{i+\frac{1}{2},j} \cdot (u_{i+1,j} - u_{i,j}) - g_{i-\frac{1}{2},j} \cdot (u_{i,j} - u_{i-1,j}) \\ &\quad + g_{i,j+\frac{1}{2}} \cdot (u_{i,j+1} - u_{i,j}) - g_{i,j-\frac{1}{2}} \cdot (u_{i,j} - u_{i,j-1}). \end{aligned}$$

Again we only want to work with the diffusivities at the midpoints $(i + \frac{1}{2}, j + \frac{1}{2})$ of the grid cells. Therefore we approximate $g_{i\pm\frac{1}{2},j}$ and $g_{i,j\pm\frac{1}{2}}$ by averaging the values of the neighbouring cell centers, e.g., $g_{i+\frac{1}{2},j} \approx \frac{1}{2}(g_{i+\frac{1}{2},j+\frac{1}{2}} + g_{i+\frac{1}{2},j-\frac{1}{2}})$. We arrive at

$$\begin{aligned} \operatorname{div}(g(|\nabla u|)\nabla u)_{i,j} &\approx \frac{1}{2} \left(g_{i+\frac{1}{2},j+\frac{1}{2}} \cdot (u_{i+1,j} + u_{i,j+1} - 2u_{i,j}) \right. \\ &\quad + g_{i+\frac{1}{2},j-\frac{1}{2}} \cdot (u_{i+1,j} + u_{i,j-1} - 2u_{i,j}) \\ &\quad + g_{i-\frac{1}{2},j+\frac{1}{2}} \cdot (u_{i-1,j} + u_{i,j+1} - 2u_{i,j}) \\ &\quad \left. + g_{i-\frac{1}{2},j-\frac{1}{2}} \cdot (u_{i-1,j} + u_{i,j-1} - 2u_{i,j}) \right). \end{aligned} \quad (15)$$

On the other hand, approximation of both gradient and divergence with respect to diagonal directions ξ , η leads to

$$\begin{aligned} \operatorname{div}(g(|\nabla u|)\nabla u)_{i,j} &\approx \frac{1}{2} \left(g_{i+\frac{1}{2},j+\frac{1}{2}} \cdot (u_{i+1,j+1} - u_{i,j}) + g_{i+\frac{1}{2},j-\frac{1}{2}} \cdot (u_{i+1,j-1} - u_{i,j}) \right. \\ &\quad \left. + g_{i-\frac{1}{2},j+\frac{1}{2}} \cdot (u_{i-1,j+1} - u_{i,j}) + g_{i-\frac{1}{2},j-\frac{1}{2}} \cdot (u_{i-1,j-1} - u_{i,j}) \right). \end{aligned} \quad (16)$$

Weighted averaging of both approximations results in

$$\begin{aligned} \operatorname{div}(g(|\nabla u|)\nabla u)_{i,j} &\approx \frac{1}{2} \left(g_{i+\frac{1}{2},j+\frac{1}{2}} \cdot (\alpha u_{i+1,j} + \alpha u_{i,j+1} + (1-\alpha)u_{i+1,j+1} - (1+\alpha)u_{i,j}) \right. \\ &\quad + g_{i+\frac{1}{2},j-\frac{1}{2}} \cdot (\alpha u_{i+1,j} + \alpha u_{i,j-1} + (1-\alpha)u_{i+1,j-1} - (1+\alpha)u_{i,j}) \\ &\quad + g_{i-\frac{1}{2},j+\frac{1}{2}} \cdot (\alpha u_{i-1,j} + \alpha u_{i,j+1} + (1-\alpha)u_{i-1,j+1} - (1+\alpha)u_{i,j}) \\ &\quad \left. + g_{i-\frac{1}{2},j-\frac{1}{2}} \cdot (\alpha u_{i-1,j} + \alpha u_{i,j-1} + (1-\alpha)u_{i-1,j-1} - (1+\alpha)u_{i,j}) \right). \end{aligned} \quad (17)$$

In the following, we consider diffusivities g defined by (4) and $\alpha = 1/2$. We set

$$\begin{aligned} \mu_{i,j,++}^k &:= \frac{1}{4}(u_{i+1,j}^k + u_{i,j+1}^k + u_{i+1,j+1}^k + u_{i,j}^k), \\ \mu_{i,j,+-}^k &:= \frac{1}{4}(u_{i+1,j}^k + u_{i,j-1}^k + u_{i+1,j-1}^k + u_{i,j}^k), \\ \mu_{i,j,-+}^k &:= \frac{1}{4}(u_{i-1,j}^k + u_{i,j+1}^k + u_{i-1,j+1}^k + u_{i,j}^k), \\ \mu_{i,j,--}^k &:= \frac{1}{4}(u_{i-1,j}^k + u_{i,j-1}^k + u_{i-1,j-1}^k + u_{i,j}^k). \end{aligned}$$

Time discretisation via an explicit Euler scheme would yield as fully discretisation of (2) the naive scheme

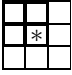
$$u_{i,j}^{k+1} = u_{i,j}^k + \tau g_{i+\frac{1}{2},j+\frac{1}{2}} \cdot (\mu_{i,j,++}^k - u_{i,j}^k) + \tau g_{i+\frac{1}{2},j-\frac{1}{2}} \cdot (\mu_{i,j,+-}^k - u_{i,j}^k) \\ + \tau g_{i-\frac{1}{2},j+\frac{1}{2}} \cdot (\mu_{i,j,-+}^k - u_{i,j}^k) + \tau g_{i-\frac{1}{2},j-\frac{1}{2}} \cdot (\mu_{i,j,--}^k - u_{i,j}^k). \quad (18)$$

Here τ denotes the time step size and $u^k = (u_{i,j}^k)_{i,j}$ the approximate solution at pixel (i, j) and time $k\tau$. Unfortunately, due to the singularity of g at zero, this scheme becomes unstable with respect to the maximum-minimum principle for arbitrary small time steps if neighbouring pixel values become arbitrary close. We use therefore a different approximation.

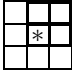
The right-hand side of (17) is exactly the average of the four approximations of $\text{div}(g\nabla u)$ in the 2×2 -pixel cells that pixel (i, j) belongs to. This inspires the following simple algorithm to compute one time step of a numerical scheme:

For each pixel (*) with coordinates (i, j) :

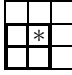
- **Consider the four cells**



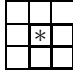
(--)



(+-)



(-+)



(++)

- **Compute the analytical solutions according to (9).**

This gives four approximations

$$u_{i,j,--}^{k+1}, u_{i,j,+-}^{k+1}, u_{i,j,-+}^{k+1}, u_{i,j,++}^{k+1}.$$

- **Average:**

$$u_{i,j}^{k+1} = \frac{1}{4}(u_{i,j,--}^{k+1} + u_{i,j,+-}^{k+1} + u_{i,j,-+}^{k+1} + u_{i,j,++}^{k+1}).$$

(19)

It is worth noting that this averaging scheme is similar to an additive operator splitting (AOS) scheme [12, 22]. One way to look at a usual AOS scheme is that it splits e.g. a two-dimensional dynamical system into two one-dimensional systems, modeling interactions in x and y directions, for which efficient numerical schemes exist. These numerical schemes are then averaged to approximate the 2D solution. Here, we split the dynamical system with right-hand side (17) into four dynamical systems belonging to four-pixel cells each of which can even be solved exactly. Again, an approximation for the solution of the full system is obtained by averaging.

Stability Analysis. The values of the analytical solution (9) at arbitrary times $t \geq 0$ are convex combinations of its initial values. By its construction from the analytical solution (9) the novel scheme (19) therefore satisfies the maximum-minimum principle. Consequently, it is absolutely stable for each τ .

Consistency Analysis. To analyse consistency, let us for simplicity focus on the TV flow, i.e., $p = 1$. Then, by (11) our final scheme reads

$$\begin{aligned}
u_{i,j}^{k+1} = & u_{i,j}^k + \tau g_{i+\frac{1}{2},j+\frac{1}{2}} \cdot (\mu_{i,j,++}^k - u_{i,j}^k) \min\{1, 1/(4\tau g_{i+\frac{1}{2},j+\frac{1}{2}})\} \\
& + \tau g_{i+\frac{1}{2},j-\frac{1}{2}} \cdot (\mu_{i,j,+ -}^k - u_{i,j}^k) \min\{1, 1/(4\tau g_{i+\frac{1}{2},j-\frac{1}{2}})\} \\
& + \tau g_{i-\frac{1}{2},j+\frac{1}{2}} \cdot (\mu_{i,j,- +}^k - u_{i,j}^k) \min\{1, 1/(4\tau g_{i-\frac{1}{2},j+\frac{1}{2}})\} \\
& + \tau g_{i-\frac{1}{2},j-\frac{1}{2}} \cdot (\mu_{i,j,--}^k - u_{i,j}^k) \min\{1, 1/(4\tau g_{i-\frac{1}{2},j-\frac{1}{2}})\}.
\end{aligned} \tag{20}$$

This scheme can be considered as a stabilisation of the explicit scheme (18). It coincides with (18), and is therefore a consistent approximation for TV diffusion, if each of the four minimum operations on its right-hand side selects the value 1. This consistency condition is fulfilled for

$$0 \leq \tau \leq \min\{1/(4g_{i+\frac{1}{2},j+\frac{1}{2}}), 1/(4g_{i+\frac{1}{2},j-\frac{1}{2}}), 1/(4g_{i-\frac{1}{2},j+\frac{1}{2}}), 1/(4g_{i-\frac{1}{2},j-\frac{1}{2}})\}.$$

For larger τ it is easy to see that linear diffusion $\partial_t u = \Delta u$ is approximated. This happens in regions where the gradient is already close to zero. In this case, however, the visual differences between linear diffusion and TV diffusion are small.

3.2 Equivalence to Shift and Rotation Invariant Wavelet Shrinkage

Ordinary single scale Haar wavelet shrinkage divides the image into disjoint 2×2 -pixel cells and performs Haar wavelet shrinkage on each of these cells as prescribed in Subsection 2.2. Unfortunately, this process is neither shift invariant nor rotation invariant. However, both properties can be achieved with a little more effort by the following procedure:

1. Shift the original image $f_{++} := (f_{i,j})$ one pixel to the right to obtain $f_{-+} := (f_{i-1,j})$, one pixel down to get $f_{+-} := (f_{i,j-1})$ and one pixel to the right and down resulting in $f_{--} := (f_{i-1,j-1})$,
2. Perform wavelet shrinkage (14) on the 2×2 cells of the four images $f_{++}, f_{-+}, f_{+-}, f_{--}$, i.e., four times ordinary Haar wavelet shrinkage.
3. Shift the resulting images back and compute the average.

Obviously, this procedure describes exactly one time step of size $\tau = \theta$ of our novel diffusion scheme (20).

4 Experiments

In Figure 1, we contrast the regularisation-free scheme (20) based on the analytical 2×2 -pixel solution for TV diffusion with a standard explicit discretisation. In this scheme, TV diffusivity is approximated by the regularised TV diffusivity $1/\sqrt{|\nabla u|^2 + \varepsilon^2}$. Since the stability condition for explicit schemes imposes to the time step size a bound which is inversely proportional to the upper bound of the



Fig. 1. **Left:** Original image, 93×93 pixels. **Middle:** TV diffusion with standard explicit scheme, where TV diffusivity is regularised with $\varepsilon = 0.01$, $\tau = 0.0025$, 10000 iterations. **Right:** TV diffusion with 2×2 -pixel scheme (20) without regularisation of diffusivity, $\tau = 0.1$, 250 iterations.

diffusivity, a high number of iterations is needed for reasonable ε . It can be seen that the 2×2 -pixel scheme and the unregularised TV diffusivity which cannot be used in the explicit scheme considerably reduce blurring effects caused by the discretisation.

Figure 2 demonstrates that although the analytically solvable case of the 2×2 -pixel cell is not the one with optimal rotational invariance, the rotational invariance is reasonable anyway.

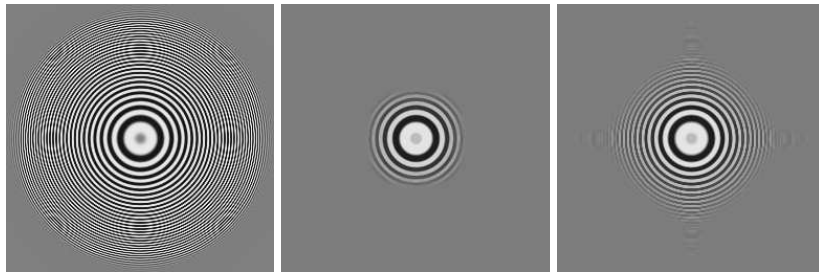


Fig. 2. **Left:** Rotationally symmetric original image, 256×256 pixels. **Middle:** TV diffusion with standard explicit scheme, $\varepsilon = 0.01$, $\tau = 0.0025$, 12000 iterations. **Right:** TV diffusion with 2×2 -pixel scheme (20), $\tau = 0.1$, 300 iterations.

Figure 3 demonstrates balanced forward–backward diffusion. With equal parameters, it can be seen again that the 2×2 -pixel scheme looks sharper by preserving finer details. Moreover, it is worth mentioning that we took a time step size that exceeded the largest admissible step size of the explicit scheme by a factor of 40.



Fig. 3. **Left:** Original image, 93×93 pixels. **Middle:** Balanced forward-backward diffusion with standard explicit scheme, $\varepsilon = 0.1$, $\tau = 0.0025$, 160000 iterations. **Right:** 2×2 -pixel scheme (20), $\tau = 0.1$, 4000 iterations.

5 Conclusion

We have introduced novel numerical schemes for a favourable class of singular nonlinear diffusion equations that includes TV and BFB diffusion. These schemes can be distinguished from other schemes by the fact that they do not require to regularise the diffusivities. They are based on analytical solutions for 4-pixel images. Combining these solutions in an AOS-like manner creates extremely simple algorithms that are absolutely stable in the maximum norm, conditionally consistent and reveal good rotation invariance. Our experiments have shown that they gives sharper results at edges than traditional schemes with regularised diffusivities, even for significantly larger time steps. This more pronounced tendency to create piecewise constant images is particularly suited for singular nonlinear PDEs.

It is our hope that this work will inspire more research on numerical schemes for PDE-based image analysis, in which analytical and numerical concepts are merged.

References

1. L. Alvarez, F. Guichard, P.-L. Lions, and J.-M. Morel. Axioms and fundamental equations in image processing. *Archive for Rational Mechanics and Analysis*, 123:199–257, 1993.
2. F. Andreu, C. Ballester, V. Caselles, and J. M. Mazón. Minimizing total variation flow. *Differential and Integral Equations*, 14(3):321–360, Mar. 2001.
3. F. Andreu, V. Caselles, J. I. Diaz, and J. M. Mazón. Qualitative properties of the total variation flow. *Journal of Functional Analysis*, 188(2):516–547, Feb. 2002.
4. G. Bellettini, V. Caselles, and M. Novaga. The total variation flow in R^N . *Journal of Differential Equations*, 184(2):475–525, 2002.
5. T. Brox, M. Welk, G. Steidl, and J. Weickert. Equivalence results for TV diffusion and TV regularisation. In L. D. Griffin and M. Lillholm, editors, *Scale-Space Methods in Computer Vision*, volume 2695 of *Lecture Notes in Computer Science*, pages 86–100, Berlin, 2003. Springer.

6. F. Catté, P.-L. Lions, J.-M. Morel, and T. Coll. Image selective smoothing and edge detection by nonlinear diffusion. *SIAM Journal on Numerical Analysis*, 32:1895–1909, 1992.
7. A. Chambolle. An algorithm for total variation minimization and applications. *Journal of Mathematical Imaging and Vision*, 20:89–97, 2004.
8. R. R. Coifman and A. Sowa. New methods of controlled total variation reduction for digital functions. *SIAM Journal on Numerical Analysis*, 39(2):480–498, 2001.
9. F. Dibos and G. Koepfler. Global total variation minimization. *SIAM Journal on Numerical Analysis*, 37(2):646–664, 2000.
10. X. Feng and A. Prohl. Analysis of total variation flow and its finite element approximations. Technical Report 1864, Institute of Mathematics and its Applications, University of Minnesota, Minneapolis, MN, July 2002. Submitted to *Communications on Pure and Applied Mathematics*.
11. S. L. Keeling and R. Stollberger. Nonlinear anisotropic diffusion filters for wide range edge sharpening. *Inverse Problems*, 18:175–190, Jan. 2002.
12. T. Lu, P. Neittaanmäki, and X.-C. Tai. A parallel splitting up method and its application to Navier–Stokes equations. *Applied Mathematics Letters*, 4(2):25–29, 1991.
13. P. Mrázek and J. Weickert. Rotationally invariant wavelet shrinkage. In B. Michaelis and G. Krell, editors, *Pattern Recognition*, volume 2781 of *Lecture Notes in Computer Science*, pages 156–163, Berlin, 2003. Springer.
14. M. Nikolova. Local strong homogeneity of a regularized estimator. *SIAM Journal on Applied Mathematics*, 61(2):633–658, 2000.
15. P. Perona and J. Malik. Scale space and edge detection using anisotropic diffusion. *IEEE Transactions on Pattern Analysis and Machine Intelligence*, 12:629–639, 1990.
16. A. Petrovic, O. Divorra Escoda, and P. Vanderghyest. Multiresolution segmentation of natural images: From linear to non-linear scale-space representations. *IEEE Transactions on Image Processing*, 13(8):1104–1114, 2004.
17. I. Pollak, A. S. Willsky, and Y. Huang. Nonlinear evolution equations as fast and exact solvers of estimation problems. *IEEE Transactions on Signal Processing*, 2004. To appear.
18. L. I. Rudin, S. Osher, and E. Fatemi. Nonlinear total variation based noise removal algorithms. *Physica D*, 60:259–268, 1992.
19. G. Steidl, J. Weickert, T. Brox, P. Mrázek, and M. Welk. On the equivalence of soft wavelet shrinkage, total variation diffusion, total variation regularization, and SIDes. *SIAM Journal on Numerical Analysis*, 42(2):686–713, 2004.
20. V. I. Tsurkov. An analytical model of edge protection under noise suppression by anisotropic diffusion. *Journal of Computer and Systems Sciences International*, 39(3):437–440, 2000.
21. J. Weickert. *Anisotropic Diffusion in Image Processing*. Teubner, Stuttgart, 1998.
22. J. Weickert, B. M. ter Haar Romeny, and M. A. Viergever. Efficient and reliable schemes for nonlinear diffusion filtering. *IEEE Transactions on Image Processing*, 7(3):398–410, Mar. 1998.